Singlet Oxygen Insertion into Hydrocarbons: The Role of First and Second-Generation Pathways in Astronomically Relevant Ices

Amit Daniely[1†], Alon Zamir[1†], Helen R. Eisenberg[1], Ester Livshits[1], Eletra Piacentino[2], Jennifer B. Bergner[3], Karin I. Öberg[2], Tamar Stein[1]

[1]Fritz Haber Research Center for Molecular Dynamics, The Hebrew University of Jerusalem, Jerusalem, 9190401, Israel.
[2]Harvard-Smithsonian Center for Astrophysics, Harvard, Cambridge, 02138, MA, USA.
[3]UC Berkeley, Department of Chemistry, Berkeley, 94720, California, USA.

[†]These authors contributed equally to this work.

Abstract

Complex organic molecules are widespread in different areas of the interstellar medium, including cold areas such as molecular clouds where chemical reactions occur in ice. The underlying molecular mechanisms responsible for the observed rich chemistry are still not understood. $O(^1D)$ atom reactions provide a pathway for chemical complexity even in cold areas, as the reactions are typically barrierless, and $O(^1D)$ is a photo-fragmented product of astronomically relevant ices such as CO_2. In this work, we use quantum chemistry methods to model reactions in astronomical ices containing oxygen with small C1 and C2 hydrocarbons in the presence of UV radiation. Our results demonstrate that the underlying molecular mechanism of reactions in ice includes the oxygen insertion reaction (first-generation reactions), photo fragmentation of products and radical recombination reactions (second-generation reactions). The mechanism explains the formation of formaldehyde in methane ice, acetaldehyde in ethane ice, CO in acetylene ice and the consumption of alcohol in all systems. This work demonstrates the important role of first and second-generation reactions in the unique chemical processes in astronomical ices; where basic molecular building blocks are fragmented and recombined into new molecules resulting in enhanced chemical complexity.

Keywords: Astrochemistry, Ab-initio molecular dynamics, oxygen insertion

1 Introduction

Molecules, including many polyatomic and complex organic molecules, are widespread throughout our universe – and observed in all stages of star and planet formation including pre-stellar cores, protostars and protoplanetary disks [1–7]. Molecules formed in these stages are incorporated in solid bodies that can be delivered to newly formed planets, providing inventory of available complex organic molecules. Thus, understanding the rich chemistry that occurs at these stages is crucial to identifying the molecules available for prebiotic chemistry and is highly important to the field of astrobiology[8].

Molecular clouds, the birthplace of stars, are shielded from external UV radiation as they contain dust particles which efficiently absorb UV radiation and thus provide a shielded environment for molecular formation. The variety of molecules observed includes complex organic molecules such as formaldehyde, acetaldehyde, methanol, vinyl alcohol, ethylene oxide, ethenone [9–14] and many more[15–21]. Molecular clouds are characterized by low temperatures and contain icy grain mantles. They also have relatively high densities in comparison to the general conditions in the diffuse interstellar medium (ISM)[8, 22]. Despite the rich chemistry taking place in molecular clouds, the underlying molecular mechanisms responsible for molecular formation in such cold dilute areas are still not understood.

In the cold cloud cores, icy grains are the major reservoir of molecules as a result of the short freeze-out time scale. Among the observed ices, water ice is the most abundant followed by carbon monoxide (CO) and Carbon dioxide (CO_2), as well as smaller amounts of organic molecules such as methane (CH_4) and methanol (CH_3OH)[23]. Gas-phase chemistry (including barrierless ion-molecule[24] and radical molecule reactions) and gas-grain chemistry are possible pathways for the production of many of the observed species[8, 25–28]. The formation of different organic molecules in environments where temperatures are greater than 30K can be explained via radical recombination mechanisms; the formation of radicals is followed by diffusion and recombination into larger molecular species[5, 29, 30].

At very low temperatures (< 20K) diffusion of some of the radical species may be limited and different low-temperature channels for organic molecule formation are expected. In cold shielded regions such as molecular clouds, external UV photons are shielded, however, the interaction of H_2 with cosmic rays results in secondary UV photons from the deexcitation of H_2 molecules (Ly-α radiation) [31]. As a result, Ly-α radiation is a dominant source of energy and the photochemical processing of ice is hypothesized to play an important role in the large variety of organic molecules observed in these areas [8, 23].

An important example is the formation of $O(^1D)$ as a result of photolysis of water (H_2O) and carbon dioxide (CO_2) ice (with efficiencies of 10% and 100% respectively.) Thus, the chemistry of $O(^1D)$ insertion reactions is a possible source of many organic reactions and provides a low-temperature pathway for organic molecule formation in those ices. Moreover, $O(^1D)$ is meta-stable with a lifetime of $\sim$110s measured[32] in the gas phase and 32s and $\sim$ 1s in neon and SF_6 in matrices, respectively[33, 34]. Thus $O(^1D)$ can efficiently diffuse in the ice before reacting and provide an efficient pathway for molecular formation in colder environments.

The gas-phase insertion reaction of O(^{1}D) has been widely studied. It has been demonstrated that the insertion of O(^{1}D) into methane is essentially barrier-less and that CH_3OH is formed; in high enough pressures it is collisionally stabilized. At lower pressures, without an efficient way to dissipate the excess energy, the molecule fragments into CH_3 + OH species [35–38].

Similar results were obtained in the gas-phase experiments of oxygen insertion into C2 hydrocarbons[39–42]. In general, the highly reactive oxygen is inserted into the hydrocarbons followed by fragmentation into radical species to dissipate the excess energy. Recently, Bergner et. al. [43, 44] studied oxygen insertion reactions in ices of astronomical relevance to obtain insights into processes taking place in ice environments under constant radiation. The ice contained CO_2 (or O_2 in the case of CH_4) with different hydrocarbons, and O(^{1}D) is produced by the photolysis of CO_2. Products obtained in ice were different from the ones obtained in the gas-phase experiments, suggesting different mechanisms are responsible for product formation in the gas-phase or ice environment. knowledge of the underlying molecular mechanism is crucial for the incorporation of the relevant reactions in astrochemical models.

In this manuscript, we model the underlying molecular pathways responsible for the rich molecular inventory of products resulting from the irradiation of ices containing different hydrocarbons and CO_2 using quantum chemistry methods. The reaction of oxygen with different hydrocarbons has been previously studied in its triplet form[41, 45–49]. Here, we focus on reactions of the hydrocarbons with oxygen in its singlet form, O(^{1}D). A possible explanation for the difference in the products in the gas phase and the ice environment is that the molecules in the ice alter the potential energy surfaces (PES) as observed previously in the case of molecular clusters [25, 26, 50, 51]. However, stability analysis of the different products on the PES reveals that while changes in stability are observed, they do not significantly alter the PES as demonstrated in the Appendix A.

Alternatively, as we demonstrate in this work, O(^{1}D) reacts directly with the available hydrocarbons (as in the gas phase), these reactions are referred to as first-generation reactions; unlike the gas phase, the ice environment provides a way to dissipate the excess energy and stabilization of the products is expected. Due to the constant irradiation of the ice, these products (as well as the C2 ice components) can further photofragment due to the interaction with UV radiation. The highly reactive radicals can further recombine, leading to new molecular species. These reactions are referred to as second-generation reactions and are demonstrated to play a role in the resulting products and their branching ratio. Thus, the observed laboratory ice chemistry is the result of a combination of O-insertion reactions, product fragmentation, and recombination of radicals, and the relative contributions of each are key to explaining and predicting astrochemical observations. Our results shed light on processes taking place in astronomical ices, where basic molecular building blocks are fragmented and recombined into new more complex molecules. To model first and secondary-generation reactions, we study the dynamics of both the ground and excited electronic states. We consider possible spin-allowed internal conversion between different electronic states and neglect the spin-forbidden inter-system crossing.

The manuscript is organized as follows: In section 2.1 we present the ground-state PESs of possible insertion reactions of $O(^1D)$ with different hydrocarbons, namely methane (CH_4), ethane (C_2H_6), ethylene (C_2H_4) and acetylene (C_2H_2); studying possible products resulting solely from $O(^1D)$ reaction with a hydrocarbon. By performing *ab-initio* molecular dynamics (AIMD) simulations on the ground electronic state we demonstrate the possible products of the reactions. We then continue to study the excited state dynamics of the available building blocks in section 2.2. The products of the insertion reactions and the building blocks of the ice, can both form radicals which are recombined to form new secondary products. Recombination products are also presented. As the reaction takes place in an ice environment, we further studied the effect of the ice on the stability of the products as reported in Appendix A. The details of all the performed calculations are given in section 3

2 Results and Discussion

2.1 Ground-state potential energy surfaces

The PESs of methane, ethane, ethylene and acetylene, with singlet oxygen, were calculated using density functional theory (DFT) (see Section 3 for details) and are shown in Figure 1. In all cases (except insertion of $O(^1D)$ into the acetylene σ bond which will be discussed below), the molecular geometry optimization of the hydrocarbon in the vicinity of $O(^1D)$ (starting from a distance of 4.9 Å) resulted in an insertion reaction of the oxygen into the hydrocarbon. The fact that the reactions are observed from optimization demonstrates that they are barrierless. To further verify that the reactions are indeed barrierless, we performed frozen PES scan calculations changing the distance between the $O(^1D)$ and the hydrocarbons. The results are shown in the supplementary material (SI) (Figure S1-S4) indicating there is no barrier along the reaction coordinate at the first stage of the $O(^1D)$ insertion. The insertion can take place via σ or π bonds. Insertion via σ bonds results in alcohols as is observed for all the systems. In cases of hydrocarbons with π bonds, namely ethylene and acetylene, barrierless formation of ethylene oxide (C_2H_4O) and oxirene (C_2H_2O) are observed, respectively. For acetylene, the frozen scan calculations exhibit a small and negligible barrier($\sim$ 2kcal/mol) in the insertion to the σ bond to form alcohol at a distance above 2Å and an angle of 180° as can be seen from Figure S1.

Figure 1 panel A shows the PES of $O(^1D)$ insertion into methane. The insertion occurs via a σ bond and the resulting product is methanol (structure b). To study the evolution of the system with time, we performed AIMD simulations using XMS-CASPT2[52, 53], details of the simulations are given in section 3 below. The simulations exhibit a fast formation of methanol in all trajectories, indicating that this is the expected product and is expected to stabilize in the ice environment. In the gas phase fragmentation is expected and indeed within the time frame of the simulations (0.5 ps), 38% of the trajectories resulted in fragmented products, namely CH_3 and OH radicals, in agreement with previous studies[35, 54, 55]. Gas-phase and liquid Argon experiments identified methanol as a major product[56]. Experiments in ice, however, resulted only in 65% methanol with the reminder as formaldehyde (CH_2O). The fact that a relatively large amount of formaldehyde was detected, which was demonstrated

to be a minor channel in gas-phase experiments implies the importance of secondary reactions taking place in the ice.

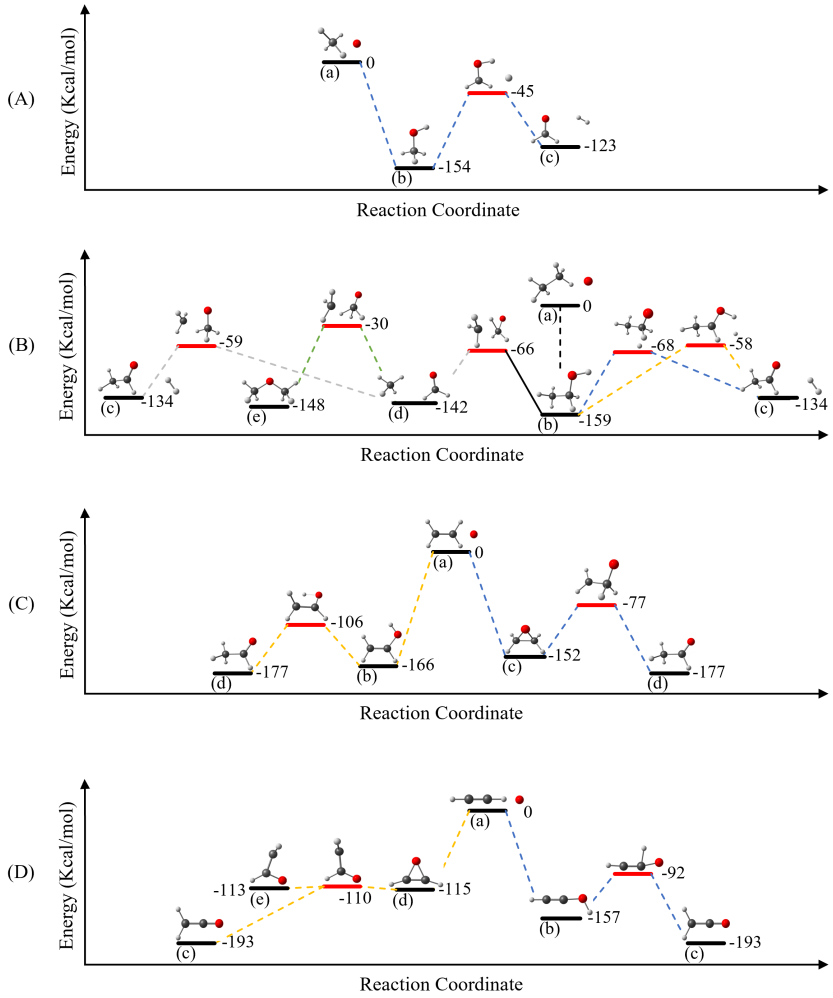

Fig. 1 PES of O(^{1}D) with (A): Methane, (B): Ethane, (C): Ethylene, (D): Acetylene. Black lines represent structures that are minima on the PES, and red lines represent transition-state structures. Different colours of the broken lines represent different pathways to the products on the PES.

Figure 1 panel B shows the PES of O(^{1}D) insertion into ethane. Here as well, only one barrierless product is observed, namely, ethanol (structure b). Other products on the PES are acetaldehyde (structure c), formaldehyde (structure d) and dimethyl ether (structure e). AIMD simulations employing XMS-CASPT2 resulted in the formation of ethanol in all trajectories. In 5% of the trajectories, we observed fragmentation of ethanol into C_2H_5 and OH radicals. The small fraction of simulations that resulted

system	product	ice experiment (%)	Estimation from gas phase ground-state simulations (%)
methane	methanol	65	100[1]
	formaldehyde	35	0
ethane	ethanol	74	100[1]
	acetaldehyde	26	0
ethylene	acetaldehyde	53	18
	ethylene oxide	47	33
	vinyl alcohol	0	49
acetylene	ethenone	100	97[2] [3]
	ethynol	0	3[3]

[1]Includes fragmented trajectories which are expected to stabilize in an ice environment.

[2]Includes fragmented trajectories and trajectories resulting in oxirene (which are expected to form ethenone in longer simulation times).

[3]Percentage from reactive trajectories.

Table 1 Comparison of branching ratio obtained by Bergner et al. and by estimation from gas phase ground-state simulations.

in fragmentation is likely due to the short simulation time (0.5 ps). The results are in agreement with reported gas-phase experiments, where the insertion takes place and then is followed by unimolecular fragmentation channels of ethanol[42, 57, 58] and with experiments in liquid Argon where alcohol is the major product [56]. H_2 or H formation channels (where acetaldehyde is formed) have been demonstrated to be minor channels[58]. The experiments in ice resulted in the formation of both ethanol and acetaldehyde with a branching ratio of ethanol 74% which again indicates that additional secondary processes are taking place.

Figure 1 panel C shows the PES of O(^{1}D) insertion into ethylene. Here there are two barrierless products resulting from the insertion reaction either from the π or the σ bonds. Reaction from the π system results in the formation of ethylene oxide (structure c) and reaction via the σ bond results in vinyl alcohol (structure b). Both structures can lead to acetaldehyde (structure d) with barriers of 75 kcal/mol from ethylene oxide and 60 kcal/mol from vinyl alcohol. XMS-CASPT2 AIMD simulations result mostly in the barrierless products namely, ethylene oxide (33%) and vinyl alcohol (46%). Acetaldehyde was observed in 18% of the simulations and 3% of the trajectories resulted in fragmentation into CH_2CH and OH radicals. Experiments in ice observed the formation of ethylene oxide and acetaldehyde with a branching ratio to ethylene oxide of 47%. Vinyl alcohol was not observed, which may be attributed to secondary reactions in which it is further photofragmented as a result of the available UV radiation.

Figure 1 panel D shows the PES of O(^{1}D) insertion into acetylene. As in the previous system, insertion can occur via the σ or π bond to form ethynol (structure b), oxirene (structure d) or formyl carbene (structure e) which can further react to form ethenone (structure c), with a negligible barrier from oxirene. The PES was also explored in the ice environment (see Appendix A for details). AIMD simulations employing XMS-CASPT2 resulted in the formation of ethenone in 58% of the simulations; among these simulations, 22% dissociated into CH_2 and CO radicals, 5% dissociated into CHCO + H. 18% of the simulations resulted in oxirene, which is likely to further react to form ethenone, as was seen in trajectories in which ethenone was

produced by passing through an oxirene product. We observe a free transition in the simulations between oxirene and formyl carbane, which is oxirene in an open form. 2% of the simulations (1 trajectory) resulted in alcohol, however, the reaction did not occur through σ insertion, but through the π system via oxirene and formyl carbene. In 22% of the simulations we did not observe any reaction taking place within the time frame of the simulations - all these trajectories occurred when the simulation starting point was from a "side" orientation - not directly above the π system. In general, in the case of ethylene and acetylene systems, reactions from the π were much favoured than those from the σ. This point is also demonstrated within the ice environment. Both for acetylene and ethylene, even when the oxygen is placed close to a hydrogen atom, the reaction takes place via the π system of the adjacent molecules, even though it is more distant, as can be seen from Figure 2.

Table 1 summarises the difference in branching ratio obtained by Bergner et al. or estimated one from gas phase ground-state simulations, demonstrating that first-generation reactions alone can not explain the experimental observation.

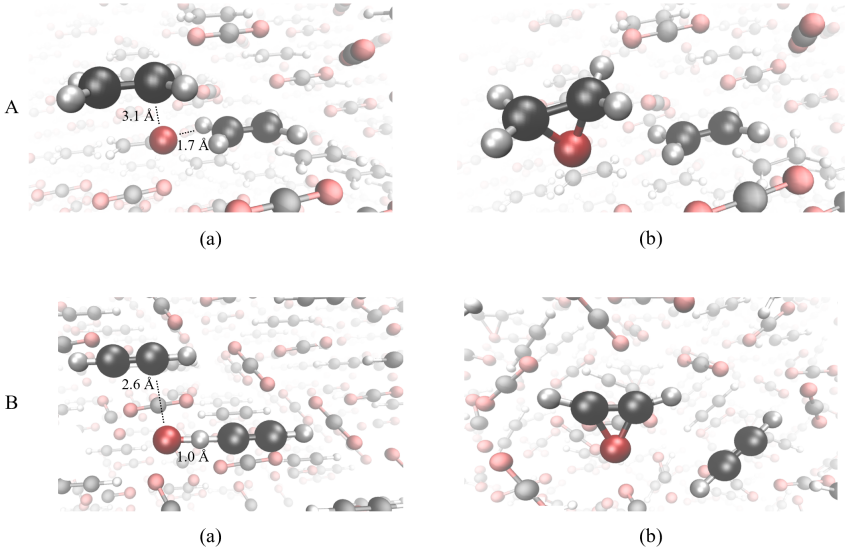

Fig. 2 Top Panel (A): (a) Initial structure of C_2H_4 with $O(^1D)$ in CO_2/C_2H_4 ice. The $O(^1D)$ is located closer to the hydrogen atom (1.7Å) than to the carbon on the neighboring C_2H_4 molecule (3.1 Å). (b): Final structure after geometric optimiztion: despite the proximity to the hydrogen, the reaction occurred via the π bond on the neighboring molecule. Bottom Panel (B): (a) Initial structure of C_2H_2 with $O(^1D)$ in CO_2/C_2H_2 ice. The $O(^1D)$ is located in a close proximity to the hydrogen (1.0 Å) than to the carbon on the neighboring C_2H_2 molecule (2.6 Å). (b): Final structure: despite the proximity to the hydrogen reaction occurred via the π bond on the neighboring molecule.

2.2 Excited states dynamics

The ice experiments performed by Bergner et al [43, 44] were performed using an ultra-high-vacuum chamber where ices are grown by introducing gases deposited on a cooled substrate (9 K) through a dosing pipe. The ice samples were irradiated using H_2D_2 lamp for 2-3 hours at different temperatures. As the ice is under constant radiation, secondary products may be formed. The hydrocarbons that constitute the ice (except methane) can absorb Ly-α radiation available in the experiment and photofragment, adding to the available collection of radicals in the ice. This is evident from the experimental results of the pure ices: irradiation of ethane leads to the formation of methane, ethylene and acetylene hydrocarbons. Irradiation of ethylene leads to the formation of ethane and acetylene, and irradiation of pure acetylene demonstrates its consumption[44]. These results indicate that in the conditions of the experiments, other components of the ice besides the CO_2 can also photofragment to form radicals and recombine and form a variety of organic species. To explore possible mechanisms we have calculated the energies of excited electronic states of the different hydrocarbons. Figure 3 shows the singlet energy levels of each hydrocarbon. As can be seen from the Figure, all the low-lying excited states of the C2 hydrocarbons are accessible (Figure 3 panels B-D) and can take part in the chemistry observed. Moreover, the products of the O(^{1}D) insertion reaction can also further photofragment and lead to secondary reactions that contribute to the chemical complexity. In the following sections, we will explore the possible products as a result of the photofragmentation of each of the hydrocarbons and the O(^{1}D) insertion products.

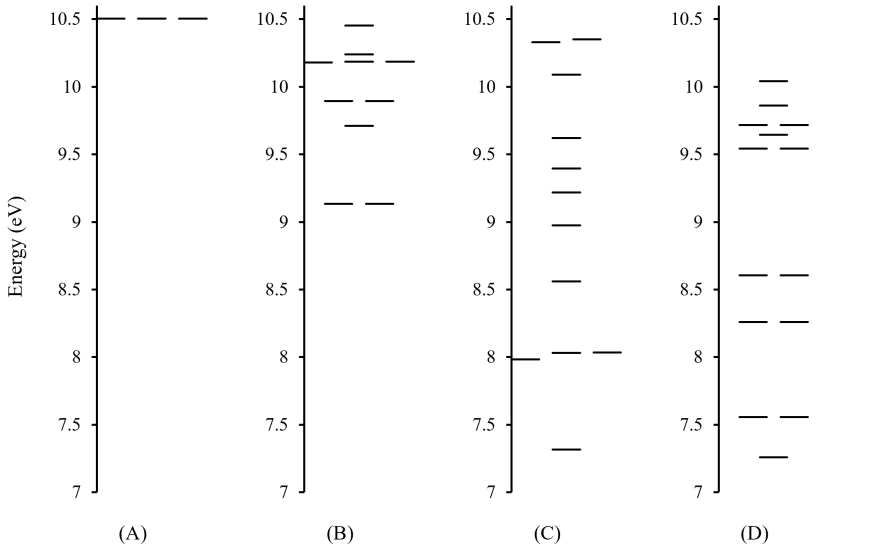

Fig. 3 Electronic excited states of (A): Methane, (B): Ethane, (C): Ethylene, (D) Acetylene calculated using EOM-CCSD/aug-cc-pVDZ.

2.2.1 CH_4 + $O(^1D)$ system

Unlike the other hydrocarbons, in methane, the lowest-lying excitation is above 10 eV which is not accessible within the energy range of the experiment, thus contributions due to methane excitations are not considered. In the presence of $O(^1D)$, methane will react to form methanol for which the ice provides an efficient way to dissipate the excess energy thus no fragmentation products are expected. Indeed, Bergner et al. did not observe any CH_3 nor OH radicals[44].

In the presence of UV radiation, the formed methanol can be excited as is evident from its energy level diagram (shown in SI Figure S5) with the lowest excited state at 6.7 eV. To study the outcome of the system upon excitation we perform Non-Adiabatic AIMD (NA-AIMD) simulations using XMS-CASPT2 on the first excited electronic state. Details of the calculations are given in section 3.2. The dynamic simulations demonstrate a quick photodissociation (within 60 fs in all 50 trajectories) of the methanol to form methoxy radical (CH_3O) and H radical. Such fragmentation of the alcohol is typical in all the systems we have studied and is in agreement with the literature[38]. As a result of the secondary reactions, H radicals are also available in the ice in addition to the $O(^1D)$ atoms. The oxygen and the hydrogen atoms are expected to efficiently diffuse even in such cold environments and will further react and recombine with other available radicals.

To study the possible recombination paths of CH_3O + H we performed ground-state AIMD simulations using DFT as detailed in section 3.1. The results of the recombination are either formaldehyde (87% of the simulations) or methanol (13% of the simulations) and depend on the starting orientation of the radicals as shown in Figure S6 in the SI. An example of trajectories is shown in Figure 4. The results explain the molecular pathway for the formation of formaldehyde, which is a result of a photofragmentation of methanol, produced when methane reacted with $O(^1D)$, followed by the recombination of the radicals formed.

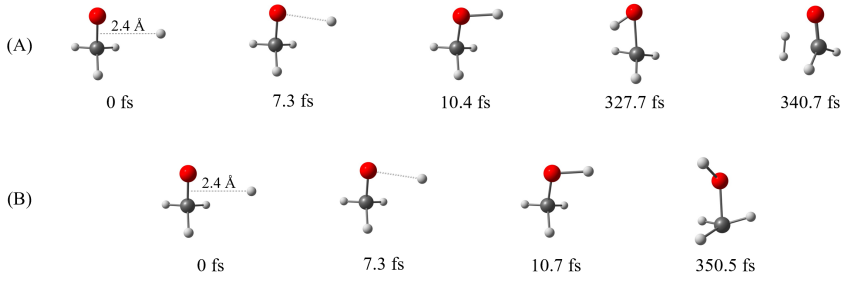

Fig. 4 Examples of the recombination between CH_3O radical and H radical. Panel A demonstrates the formation of formaldehyde and H_2. Panel B demonstrates the formation of methanol.

2.2.2 C_2H_6 + $O(^1D)$ system

Bergner et al.[44] found that oxygen atoms react with ethane to form ethanol and acetaldehyde, with a branching ratio to ethanol of 74%, while ground-state dynamics demonstrate solely the formation of ethanol. Unlike in the gas phase, in the ice environment, the ethanol can be stabilized and not fragmented. The calculation of excited state energies of ethanol shown in Figure S7 in the SI, demonstrates that ethanol can be excited under experimental conditions. To study the results of its photoexcitation, we perform NA-AIMD simulations using XMS-CASPT2 on the first excited electronic state. Ethanol in the first excited state fragments very quickly into ethoxy radical (CH_3CH_2O) radical and H radical in all 50 trajectories.

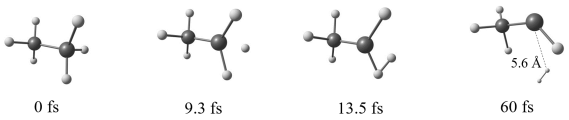

Fig. 5 Example of a trajectory starting from the second low-lying excited state of ethane resulting in ethylidene + H_2

Ethane, the main component of the ice can also photofragment under the experimental conditions as is evident from its energy level diagram in Figure 3 panel B. For ethane, we performed NA-AIMD simulations using XMS-CASPT2 on the two lowest-lying excited electronic states. Starting from each state, namely S1 or S2, we run 50 trajectories for 60 fs as by this time all the trajectories resulted in the fragmented products. The statistics are similar for both initial states and so are independent of the starting electronic state as demonstrated in Figure S8 in the SI. The reason is that when starting on S2, the system rapidly crosses to S1, where ethylidene (CH_3CH), is formed. In total, 96% of the trajectories resulted in ethylidene (CH_3CH) and H_2 and 4% resulted in ethyl radical (CH_3CH_2) + H. An example trajectory is demonstrated in Figure 5. Both H and H_2 loss have been reported as possible fragmentation pathways of ethane[59–61], and the formation of ethylidene has been previously discussed[62, 63]. It has been suggested to be produced from the reaction of $C(^1D)$ with methane [64] and via the reaction between $O(^3P)$ and propene under combustion[65]. Additionally, ethylidene has been observed as a bound species on the surface of platinum [66] and as part of transition metal complexes[67]. Free ethylidene has recently been produced in the photodissociation of gaseous methylketene and propenal, while the triplet form of ethylidene has been demonstrated as stable in the absence of collisions, the singlet form undergoes isomerization by a 1,2-hydrogen atom shift producing vibrationally excited ethylene[68]. In the ice experiment, the irradiation of pure ethane ice results in ethylene among other products; the route is likely to go through the singlet ethylidene product, which is the main product of photofragmentation of ethane, which undergoes a fast H atom migration to form ethylene [68].

In addition to the presence of $O(^1D)$ in the ice, photofragmentation of both ethanol and ethane results in highly reactive species in close proximity to each other. Their high reactivity can lead to the recombination of radical species, especially with the

presence of oxygen and hydrogen that can effectively diffuse in the ice even at low temperatures. To study the recombination processes of the radicals, we performed DFT AIMD simulations sampling different initial orientations of the radicals, with the final result depending on the initial orientations. Interestingly, the major product of the recombination is acetaldehyde (53.7%), followed by the formation of formaldehyde (31.7%) and ethanol (14.6%), as can be seen in Figure S9 in the SI. The recombination processes can explain the pathway for acetaldehyde formation, which is the second major product observed in the experiment.

2.2.3 C_2H_4 + $O(^1D)$ system

Ground-state simulations of $O(^1D)$ reacting with ethylene predicted 45% formation of vinyl alcohol, 33% formation of ethylene oxide and only 18% formation of acetaldehyde, while Bergner et al[44] observed the formation of acetaldehyde (53%) and ethylene oxide (47%) with no observation of vinyl alcohol. Vinyl alcohol was however observed in different experiments, thus it is possible that vinyl alcohol was formed in the ice, and further photofragmented as a result of the available UV radiation[69]. Electronic energy levels of vinyl alcohol are presented in Figure S10 in the SI, demonstrating that like the other alcohols under study, excited electronic states are accessible within experimental conditions.

We have used XMS-CASPT2 to study the fate of vinyl alcohol as a result of interaction with radiation and performed NA-AIMD simulations on its first excited state. In all the simulations we observed a quick fragmentation of excited vinyl alcohol into vinyloxy radical (CH_2CHO) and H radical.

To model the recombination of the radicals, we perform DFT AIMD simulation starting from different orientations on the ground state. The majority of trajectories (70.8%) result in the formation of the observed product, namely acetaldehyde. The rest of the simulations resulted in vinyl alcohol (12.9%) or ethenone (14.6%) as shown in Figure S11 in the SI. While ethylene oxide is formed on the ground state, second-generation reactions are needed to explain the formation route of acetaldehyde via the consumption of vinyl alcohol.

The ice components can also absorb radiation as is evidenced by the electronic energy levels in Figure 3 panel C. To study possible fragmentation paths due to radiation, we performed NA-AIMD simulations using XMS-CASP2 on the first and second excited electronic states of the hydrocarbon. The photodynamics of ethylene are well-studied[70–73]. The S1 state, the Rydberg state, was not reactive and all simulations resulted in a distorted form of ethylene. In S2, the $\pi\pi^*$ state, only 10% of the simulations resulted in a chemical change in the time frame of the simulations: we observed the formation of ethylidene CH_3CH (1 trajectory) and dissociation into vinyl radical and H radical, $CHCH_2$ + H (2 trajectories) and acetylene + H_2 (2 trajectories). These trajectories demonstrate the formation of acetylene from ethylene which is observed in the pure ice experiments and is consistent with the observation that upon irradiation of ethane and ethylene ice, acetylene is formed. In the rest of the simulations, state S2 stayed as C_2H_4 and rotated around the π bond during the simulations. We observed hopping between S2/S1 states in a twisted geometry of ethylene and between S1/S0 in twisted-pyramidalized ethylene in agreement with the literature[70–72]. Ethylene in

its rotated form is more stable in the triplet state, and possibly inter-system crossing can also take place [74].

2.2.4 C_2H_2 + $O(^1D)$ system

From the ground-state dynamics of acetylene and oxygen, we expect ethenone to be the major product. Bergner at al [44] observed ethenone and CO as the reaction products. While ethenone is directly formed from the reaction between acetylene and $O(^1D)$, the pathway to form the large quantities of the observed CO was not clear and one of the possible suggested explanations was that it resulted from second-generation reactions of the hydrocarbon fragments and $O(^1D)$. To study possible second-generation reactions we performed NA-AIMD simulations using XMS-CASPT2 starting from the S1, S2 and S3 low-lying excited electronic states of acetylene. We ran 50 trajectories, each for 300 fs. The product distribution is presented in Figure 6.

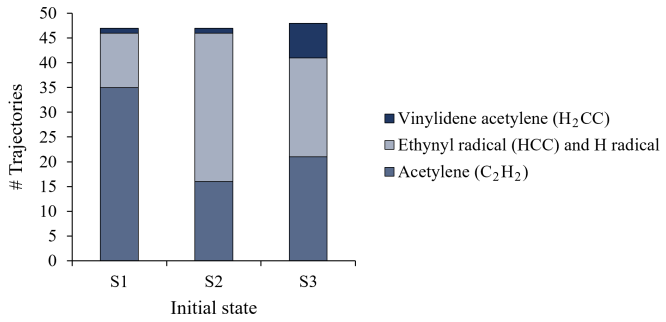

Fig. 6 Product distribution calculated from NA-AIMD simulations of photoexcited acetylene, starting from different electronic states.

In the starting structure of linear acetylene, the three states are very close in energy as is demonstrated in Figure 3 panel (D). We allow crossing between all three excited states and the ground state and indeed we observed crossing between all the excited states. In the excited states, the structure of acetylene is distorted and we get the cis and trans isomers which have been previously identified [75, 76]. We observed the photodissociation channel of acetylene into ethynyl radical (HCC) and H radical, which occurred mainly in the S1 and S2 states. This channel has been previously reported as a fragmentation channel of acetylene [59, 77–81]. Additionally, we observed the formation of the methylidenecarbene (H_2CC) product in 6% of all simulations. This structure has been identified as the minimum on the S1 PES [76]. The formation of this product is obtained via two possible pathways. In the first pathway, the system crosses back to the ground state in a distorted form where the acetylene is no longer linear. The distortion enables hydrogen transfer from one carbon to the other on the ground state leading to methylidenecarbene (H_2CC) formation. As the product is vibrationally excited when crossing back to the ground state, the hydrogen can also move back to re-form acetylene and the transition between acetylene to methylidenecarbene (H_2CC)

is observed through the rest of the dynamics. In the second pathway, the formation of methylidenecarbene (H_2CC) occurs in the S1 state and the product is stable: no reformation of acetylene is observed.

The available radicals in the ice can further react with O(^{1}D), and we studied the recombination process of ethynyl radical (HCC) with O(^{1}D), using DFT AIMD simulations as in the previous systems. The majority of the simulations resulted in fragmentation to HC and CO radicals, explaining the formation path of CO observed in the experiment. Examples of trajectories are demonstrated in Figure 7.

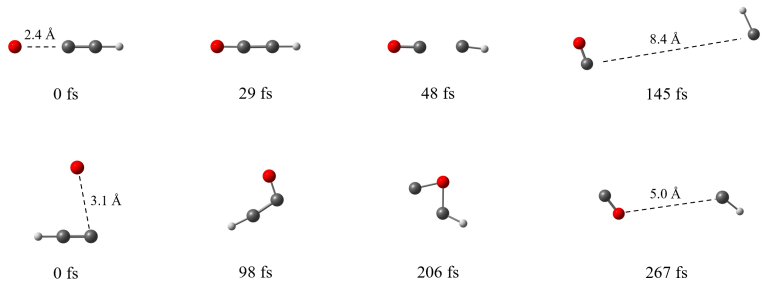

Fig. 7 Examples of AIMD simulations of the reaction between HCC and oxygen (^{1}D).

3 Methods

3.1 Ground state

PES of the O(^{1}D) insertion reactions into different hydrocarbons were performed using DFT with the Q-Chem 5 software package[82]. The different structures on the PES were optimized using the ωB97X-V functional [83] with an aug-cc-pVDZ basis set[84]. Transition state structures were studied by using the freezing string method (FSM) [85] and intrinsic reaction coordinate (IRC). Frequency calculations were performed to verify that all the structures on the PESs are indeed minimum points or saddle points. For more accurate energies, we performed single-point calculations on all the optimal structures on the PESs using the ωB97X-V functional [83] with an aug-cc-pVTZ basis set.

To study the evolution of the systems with time, we performed AIMD simulations of the O(^{1}D) insertion reactions into the different hydrocarbons in the study. AIMD simulations were carried out with the extended multi-state complete active space second-order perturbation theory (XMS-CASPT2) method [52, 53] within the so-called "left SS-SR" [86] contraction scheme for internally contracted basis functions where a vertical shift set to 0.2 E_h was used. The dynamic simulations on the ground-state surface were done using the BAGEL electronic structure package[87] interfaces with the Newton-X (v2.2.0) program.[88] The simulations ran for 500 fs using a time-step of 0.3 fs.

1. Methane: For the CH_4 system, we used a (10e,8o) active space. We ran 60 trajectories starting from two possible initial positions; 30 trajectories started from an orientation where the $O(^1D)$ is located in front of a hydrogen atom and the other 30 trajectories started where the oxygen is positioned between two hydrogen atoms.
2. Ethane: For the C_2H_6 system, we used a (12e,8o) active space. We ran 60 trajectories starting from two different initial positions; 30 trajectories started from an orientation where the $O(^1D)$ is located on the side of the molecule, facing a hydrogen atom. The other 30 trajectories started where the oxygen is positioned above the two carbon atoms.
3. Ethylene: For the CH_2CH_2 system, we performed AIMD simulations on the ground state using a (10e,8o) active space. We started the simulation from three starting points: where the $O(^1D)$ is in front of the π bond in the molecular plane and perpendicular to the molecular plane. Additionally, we have started the simulations from a σ direction where the $O(^1D)$ is located between two hydrogen atoms.
4. Acetylene: For the acetylene system, we performed AIMD simulations on the ground state using a (10e,7o) active space. To model the insertion reaction from the π direction we started the simulation where the $O(^1D)$ is located in front of the middle of the π bond perpendicular to the molecular plane. Alternatively, we have modelled the reaction starting from the σ direction. When $O(^1D)$ is placed along the axis of the acetylene molecule (i.e the CH-O angle is 180° degrees) we observed distancing of $O(^1D)$ at the time scale of the simulations. We then sampled this direction by placing the $O(^1D)$ at different angles from the acetylene molecule (specifically the CH-O angle) varying from 100° to 170°.

In all systems, the nuclear velocities were randomly sampled from the Maxwell-Boltzmann distribution according to the temperature which varied between 30K - 80K in all trajectories.

3.2 Excited-states

Excitation energies were calculated using the equation of motion Coupled-Cluster singles doubles (EOM-CCSD)[89–92] method and XMS-CASPT2[52, 53]. To study different reactions in excited electronic states and their propagation in time, we performed NA-AIMD simulations using the XMS-CASPT2 method [52, 53] within the so-called " left SS-SR " [86] contraction scheme for internally contracted basis functions where a vertical shift set to 0.2 E_h was used similar to the ground-state calculations. We performed XMS-CASPT2 NA-AIMD with an aug-cc-pVDZ basis set utilizing the BAGEL electronic structure package[87] interfaced with the Newton-X (v2.2.0) program[88]. In the excited state dynamics, we take into account non-adiabatic transitions between different states by allowing surface hopping[93]. The initial conditions of each trajectory (namely geometry and velocity) were generated from a DFT AIMD simulation on the ground state of each system at 30K. We sampled initial conditions every 40 steps starting from step 580 fs assuming that by this time the system reached thermalization. For each state, we ran 50 trajectories each for 300 fs or until fragmentation occurred, using 0.3 fs time step.

1. Ethane: we performed XMS-CASPT2 calculations with a (6e,8o) active space. Simulations were performed starting on the first two excited states, namely S1 and S2 allowing non-adiabatic transitions only between sequential states.
2. Ethylene: we performed XMS-CASPT2 calculations for the first two excited states, namely S1 and S2. We used a (8e,6o) active space when performing dynamic simulations on the first excited state taking into account non-adiabatic coupling between the ground state and the first excited state. On S2 we used a (8e,8o) active space while taking into account non-adiabatic transitions between sequential states S0, S1, S2 and S3.
3. Acetylene: we performed NA-AIMD simulations starting with the S1, S2 and S3 low-lying excited states employing XMS-CASPT2 with a (6e,6o) active space. Non-adiabatic coupling between all states (three excited states and the ground state) was allowed during the simulations.
4. Alcohols: namely methanol, ethanol and vinyl-alcohol. We have performed NA-AIMD simulations on the S1 state and allowed surface-hopping back to the ground state. We observed a rapid fragmentation of the OH bond in all cases, thus all the simulations ran for 60 fs. For methanol, we used XMS-CASPT2 with a (4e,6o) active space using three states for the state average (including the ground state). For ethanol, we used XMS-CASPT2 with a (6e,8o) active space using three states for the state average (including the ground state). For vinyl-alcohol, we used XMS-CASPT2 with a (4e,8o) active space.

3.3 Radical recombination

Due to the high computational cost of the XMS-CASPT2 method, we performed AIMD simulations to study the recombination processes using DFT, specifically with the ωB97X-V functional and an aug-cc-pVDZ basis set. We started with two species at a distance of 4Å from the centre of the carbon bond and sampled different angles between the fragmented products. For each angle, we ran 30 trajectories with varying temperatures between 10K - 40K and the velocities were randomly sampled from the corresponding Maxwell-Boltzmann distribution.

3.4 Ice environment

To study the effect of the ice environment on the stability of the different structures, calculations were performed within the framework DFT, using the plane-wave-based Vienna *ab-initio* simulation package (VASP)[94] with PAW[95, 96] pseudopotentials, and the PBE0 [97–99] hybrid exchange-correlation functional. Due to significant Van der Waals interactions between the molecules, Van der Waals dispersion corrections were calculated using the many-body dispersion energy method of Tkatchenko et al. [100, 101] Results were converged to an accuracy of approximately 0.03 eV, in relation to the cutoff energy for the plane-wave basis (converged at 400 eV), the k-point mesh density and the vacuum length in the calculations for isolated molecules. Structures were relaxed using ionic relaxation with the conjugate gradient algorithm.

4 Conclusion

The reaction of $O(^1D)$ with different hydrocarbons is barrierless and results in the addition of oxygen to the π bond or in insertion into the CH bond. In the gas phase, without an efficient way to dissipate the excess energy, the products are mainly fragmentation products. In contrast, in an ice environment, the ice supplies an efficient way to dissipate the excess energy and stabilization of the products is obtained. Our results demonstrate that when the ice is exposed to UV radiation, as expected in areas such as molecular clouds, second-generation reactions, where the products further photodissociate into radicals and then recombine, play a key role and add to the chemical complexity. In the case of methane we demonstrate that while methanol is formed in a direct insertion reaction, the formation of formaldehyde is a result of photofragmentation of the methanol into radicals; their recombination provides a path for formaldehyde formation. In the case of ethane and ethylene, second-generation reactions are responsible for the formation of acetaldehyde, and in the case of acetylene, the second-generation reactions lead to the formation of CO which was observed in large quantities in the experiments.

Supplementary information. If your article has accompanying supplementary file/s please state so here.

Acknowledgments. T. S. acknowledges a European Research Council (ERC) Grant No. 101115429, AstroMol.

Appendix A The effect of the ice on the structure's stability

In order to understand and quantify the effect of the ice on the carbohydrate molecule of interest calculations of energy and atomic configuration were performed for both the isolated molecule in a vacuum and the molecule within the hydrocarbon/CO_2 ice. All energies are given with reference to the isolated oxygen atom and the isolated hydrocarbon molecule or the hydrocarbon/CO_2 ice, for the vacuum and ice calculations respectively. All calculations were performed with spin polarization. The initial magnetization was set to zero in structures that otherwise reached the triplet state in order to ensure a singlet state as this is the system of interest. The ice was built for each hydrocarbon molecule by creating a small unit cell with the hydrocarbon molecule and 2 CO_2 molecules. The ice was then relaxed using ionic relaxation while allowing the cell volume and shape to also relax. A supercell was then created by replicating the small relaxed unit cell in the direction of each lattice vector, thereby creating a supercell of fixed dimensions with 8 replicated hydrocarbon molecules and 16 CO_2 molecules. One hydrocarbon molecule in the supercell was then replaced by the carbohydrate molecule of interest and the ice was relaxed to obtain the energies and atomic configurations of the stable states. This was carried out for various orientations of the carbohydrate with the ice. The energies and atomic configurations of the transition states were calculated by fixing the atomic positions of the transition state of the carbohydrate molecule of interest to those obtained in section 2.1 and relaxing

the rest of the ice. Binding energies were also determined by calculating the difference between the energy of the ice-carbohydrate complex and the single-point energy of the ice with the carbohydrate removed plus the single-point energy of the carbohydrate with the ice removed. Additionally, the effect of having one CO_2 molecule per hydrocarbon rather than two was studied and found to not have a significant effect. As can be seen, the ice always stabilizes the carbohydrate more than the vacuum, as a result of hydrogen bonding between the oxygen atom and the ice. Oxirene and ethynol are more stabilized by the ice than ethenone due to greater hydrogen bonding with the ice, however, this is not a significant effect. There were many meta-stable states observed for each carbohydrate molecule depending on the initial orientation of the molecule within the ice. Note that the same effect was observed when an oxygen radical was introduced into the hydrocarbon/CO_2 ice and the system was relaxed resulting in the oxygen atom bonding with a hydrocarbon. The resulting carbohydrate is orientated differently within the ice depending on the initial placement of the oxygen radical with the ice. The binding energy calculations show that most of the difference in energy of these metastable states results from the reorganization of the ice around the carbohydrate and not from significant differences in the bonding between the carbohydrate and the ice.

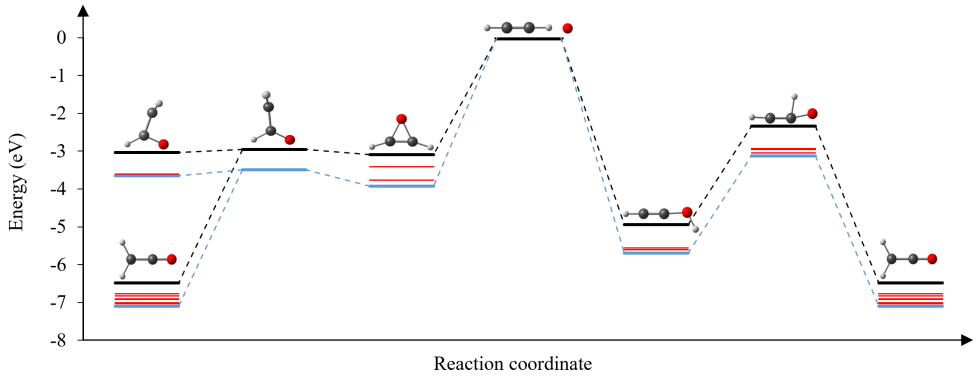

Fig. A1 Comparison of the stability of the different structures on the acetylene PES calculated in vacuum (black lines) and in different orientations of the ice (red lines), the most stable orientation in the ice is represented in blue

References

[1] Öberg, K.I., Bottinelli, S., Jørgensen, J.K., Van Dishoeck, E.F.: A cold complex chemistry toward the low-mass protostar b1-b: evidence for complex molecule production in ices. The Astrophysical Journal **716**(1), 825 (2010)

[2] Bacmann, A., Taquet, V., Faure, A., Kahane, C., Ceccarelli, C.: Detection of complex organic molecules in a prestellar core: a new challenge for astrochemical models. Astronomy & Astrophysics **541**, 12 (2012)

[3] Dishoeck, E.F., Blake, G.A., Jansen, D.J., Groesbeck, T.: Molecular abundances and low-mass star formation. ii. organic and deuterated species toward iras 16293-2422. Astrophysical Journal **447**(2), 760–782 (1995)

[4] Öberg, K.I., Guzmán, V.V., Furuya, K., Qi, C., Aikawa, Y., Andrews, S.M., Loomis, R., Wilner, D.J.: The comet-like composition of a protoplanetary disk as revealed by complex cyanides. Nature **520**(7546), 198–201 (2015)

[5] Herbst, E., Van Dishoeck, E.F.: Complex organic interstellar molecules. Annual Review of Astronomy and Astrophysics **47**, 427–480 (2009)

[6] Öberg, K.I., Bergin, E.A.: Astrochemistry and compositions of planetary systems. Physics Reports **893**, 1–48 (2021)

[7] Jørgensen, J.K., Belloche, A., Garrod, R.T.: Astrochemistry during the formation of stars. Annual Review of Astronomy and Astrophysics **58**, 727–778 (2020)

[8] Sandford, S.A., Nuevo, M., Bera, P.P., Lee, T.J.: Prebiotic astrochemistry and the formation of molecules of astrobiological interest in interstellar clouds and protostellar disks. Chemical reviews **120**(11), 4616–4659 (2020)

[9] Snyder, L.E., Buhl, D., Zuckerman, B., Palmer, P.: Microwave detection of interstellar formaldehyde. Physical Review Letters **22**(13), 679 (1969)

[10] Gordon, M.A., Snyder, L.E.: Molecules in the galactic environment. Molecules in the Galactic Environment (1973)

[11] Ball, J.A., Gottlieb, C.A., Lilley, A., Radford, H.: Detection of methyl alcohol in sagittarius. Astrophysical Journal, vol. 162, p. L203 **162**, 203 (1970)

[12] Turner, B.E., Apponi, A.J.: Microwave detection of interstellar vinyl alcohol, ch2= choh. The Astrophysical Journal **561**(2), 207 (2001)

[13] Dickens, J., Irvine, W.M., Ohishi, M., Ikeda, M., Ishikawa, S., Nummelin, A., Hjalmarson, Å.: Detection of interstellar ethylene oxide (c-c2h4o). The astrophysical journal **489**(2), 753 (1997)

[14] Turner, B.: Microwave detection of interstellar ketene. Astrophysical Journal, Part 2-Letters to the Editor, vol. 213, Apr. 15, 1977, p. L75-L79. **213**, 75–79 (1977)

[15] Müller, H.S.: Molecules in space. Encyclopedia of Astrobiology, 1863 (2015)

[16] McGuire, B.A.: 2018 census of interstellar, circumstellar, extragalactic, protoplanetary disk, and exoplanetary molecules. The Astrophysical Journal Supplement Series **239**(2), 17 (2018)

[17] McGuire, B.A., Loomis, R.A., Burkhardt, A.M., Lee, K.L.K., Shingledecker, C.N., Charnley, S.B., Cooke, I.R., Cordiner, M.A., Herbst, E., Kalenskii, S., *et al.*: Detection of two interstellar polycyclic aromatic hydrocarbons via spectral matched filtering. Science **371**(6535), 1265–1269 (2021)

[18] Burkhardt, A.M., Lee, K.L.K., Changala, P.B., Shingledecker, C.N., Cooke, I.R., Loomis, R.A., Wei, H., Charnley, S.B., Herbst, E., McCarthy, M.C., *et al.*: Discovery of the pure polycyclic aromatic hydrocarbon indene (c-c9h8) with gotham observations of tmc-1. The Astrophysical Journal Letters **913**(2), 18 (2021)

[19] Cernicharo, J., Agúndez, M., Cabezas, C., Tercero, B., Marcelino, N., Pardo, J.R., De Vicente, P.: Pure hydrocarbon cycles in tmc-1: Discovery of ethynyl cyclopropenylidene, cyclopentadiene, and indene. Astronomy & Astrophysics **649**, 15 (2021)

[20] Sita, M.L., Changala, P.B., Xue, C., Burkhardt, A.M., Shingledecker, C.N., Lee, K.L.K., Loomis, R.A., Momjian, E., Siebert, M.A., Gupta, D., *et al.*: Discovery of interstellar 2-cyanoindene (2-c9h7cn) in gotham observations of tmc-1. The Astrophysical Journal Letters **938**(2), 12 (2022)

[21] Loru, D., Cabezas, C., Cernicharo, J., Schnell, M., Steber, A.L.: Detection of ethynylbenzene in tmc-1 and the interstellar search for 1, 2-diethynylbenzene. Astronomy & Astrophysics **677**, 166 (2023)

[22] Benson, P., Myers, P.: A survey for dense cores in dark clouds. Astrophysical Journal Supplement Series (ISSN 0067-0049), vol. 71, Sept. 1989, p. 89-108. Research supported by the American Astronomical Society, Dudley Observatory, and William and Flora Hewitt Foundation. **71**, 89–108 (1989)

[23] Öberg, K.I.: Photochemistry and astrochemistry: Photochemical pathways to interstellar complex organic molecules. Chemical reviews **116**(17), 9631–9663 (2016)

[24] Agúndez, M., Wakelam, V.: Chemistry of dark clouds: databases, networks, and models. Chemical Reviews **113**(12), 8710–8737 (2013)

[25] Jose, J., Zamir, A., Stein, T.: Molecular dynamics reveals formation path of benzonitrile and other molecules in conditions relevant to the interstellar medium. Proceedings of the National Academy of Sciences **118**(19), 2101371118 (2021)

[26] Zamir, A., Stein, T.: Isomerization of hydrogen cyanide and hydrogen isocyanide in a cluster environment: quantum chemical study. The Journal of Chemical Physics **156**(5) (2022)

[27] Kaiser, R.I.: Experimental investigation on the formation of carbon-bearing molecules in the interstellar medium via neutral- neutral reactions. Chemical Reviews **102**(5), 1309–1358 (2002)

[28] Parker, D.S., Zhang, F., Kim, Y.S., Kaiser, R.I., Landera, A., Kislov, V.V., Mebel, A.M., Tielens, A.: Low temperature formation of naphthalene and its role in the synthesis of pahs (polycyclic aromatic hydrocarbons) in the interstellar medium. Proceedings of the National Academy of Sciences **109**(1), 53–58 (2012)

[29] Garrod, R.T., Weaver, S.L.W., Herbst, E.: Complex chemistry in star-forming regions: An expanded gas-grain warm-up chemical model. The Astrophysical Journal **682**(1), 283 (2008)

[30] Bera, P.P., Stein, T., Head-Gordon, M., Lee, T.J.: Mechanisms of the formation of adenine, guanine, and their analogues in uv-irradiated mixed nh3: H2o molecular ices containing purine. Astrobiology **17**(8), 771–785 (2017)

[31] Prasad, S.S., Tarafdar, S.P.: Uv radiation field inside dense clouds-its possible existence and chemical implications. Astrophysical Journal, Part 1 (ISSN 0004-637X), vol. 267, April 15, 1983, p. 603-609. NASA-supported research. **267**, 603–609 (1983)

[32] Sharpee, B., Slanger, T.: O (1d2-3p2, 1, 0) 630.0, 636.4, and 639.2 nm forbidden emission line intensity ratios measured in the terrestrial nightglow. The Journal of Physical Chemistry A **110**(21), 6707–6710 (2006)

[33] Fournier, J., Mohammed, H., Deson, J., Maillard, D.: Vacuum uv photolysis of co2. rare-gas oxide formation in matrices. Chemical Physics **70**(1-2), 39–45 (1982)

[34] Mohammed, H.H.: O (1 d) lifetime shortening in sf6 matrix. The Journal of chemical physics **93**(1), 412–415 (1990)

[35] DeMore, W.B., Raper, O.: Reaction of o (1 d) with methane. The Journal of Chemical Physics **46**(7), 2500–2505 (1967)

[36] Lin, C., DeMore, W.: Reactions of atomic oxygen (1d) with methane and ethane. The Journal of Physical Chemistry **77**(7), 863–869 (1973)

[37] Hays, B.M., Wehres, N., DePrince, B.A., Roy, A.A., Laas, J.C., Weaver, S.L.W.: Rotational spectral studies of o (1d) insertion reactions with methane and ethylene: Methanol and vinyl alcohol in a supersonic expansion. Chemical Physics Letters **630**, 18–26 (2015)

[38] Lin, J., Harich, S., Lee, Y., Yang, X.: Dynamics of the o (1 d)+ ch 4 reaction: Atomic hydrogen channel vs molecular hydrogen channel. The Journal of chemical physics **110**(22), 10821–10829 (1999)

[39] González, M., Puyuelo, M.P., Hernando, J., Martínez, R., Sayós, R., Enríquez, P.A.: Nascent oh (x2π) product state distributions from the reaction of o (1d) with ethylene.: A laser-induced fluorescence study. Chemical physics letters **346**(1-2), 69–80 (2001)

[40] Honma, K.: Reaction of o (1 d) with ethylene: Vibrational and rotational state distribution of product oh. The Journal of chemical physics **99**(10), 7677–7686 (1993)

[41] Lee, S.-H., Chen, W.-K., Huang, W.-J.: Exploring the dynamics of reactions of oxygen atoms in states p3 and d1 with ethene at collision energy 3 kcal mol- 1. The Journal of chemical physics **130**(5) (2009)

[42] Nuñez-Reyes, D., Hickson, K.M.: Rate constants and h-atom product yields for the reactions of o (1d) atoms with ethane and acetylene from 50 to 296 k. The Journal of Physical Chemistry A **122**(20), 4696–4703 (2018)

[43] Bergner, J.B., Öberg, K.I., Rajappan, M.: Methanol formation via oxygen insertion chemistry in ices. The Astrophysical Journal **845**(1), 29 (2017)

[44] Bergner, J.B., Öberg, K.I., Rajappan, M.: Oxygen atom reactions with c2h6, c2h4, and c2h2 in ices. The Astrophysical Journal **874**(2), 115 (2019)

[45] Bennett, C.J., Osamura, Y., Lebar, M.D., Kaiser, R.I.: Laboratory studies on the formation of three c2h4o isomers—acetaldehyde (ch3cho), ethylene oxide (c-c2h4o), and vinyl alcohol (ch2choh)—in interstellar and cometary ices. The Astrophysical Journal **634**(1), 698 (2005)

[46] Girard, Y., Chaquin, P.: Addition reactions of 1d and 3p atomic oxygen with acetylene. potential energy surfaces and stability of the primary products. is oxirene only a triplet molecule? a theoretical study. The Journal of Physical Chemistry A **107**(48), 10462–10470 (2003)

[47] Zuo, J., Chen, Q., Hu, X., Guo, H., Xie, D.: Dissection of the multichannel reaction of acetylene with atomic oxygen: from the global potential energy surface to rate coefficients and branching dynamics. Physical Chemistry Chemical Physics **21**(3), 1408–1416 (2019)

[48] Fu, B., Han, Y.-C., Bowman, J.M., Angelucci, L., Balucani, N., Leonori, F., Casavecchia, P.: Intersystem crossing and dynamics in o (3p)+ c2h4 multichannel reaction: Experiment validates theory. Proceedings of the National Academy of Sciences **109**(25), 9733–9738 (2012)

[49] Pokhilko, P., Shannon, R., Glowacki, D., Wang, H., Krylov, A.I.: Spin-forbidden channels in reactions of unsaturated hydrocarbons with o (3p). The Journal of Physical Chemistry A **123**(2), 482–491 (2018)

[50] Rossich Molina, E., Stein, T.: The effect of cluster size on the intra-cluster ionic polymerization process. Molecules **26**(16), 4782 (2021)

[51] Stein, T., Jose, J.: Molecular formation upon ionization of van der waals clusters and implication to astrochemistry. Israel Journal of Chemistry **60**(8-9), 842–849 (2020)

[52] Shiozaki, T., Győrffy, W., Celani, P., Werner, H.-J.: Communication: Extended multi-state complete active space second-order perturbation theory: Energy and nuclear gradients. The Journal of Chemical Physics **135**(8) (2011)

[53] Granovsky, A.A.: Extended multi-configuration quasi-degenerate perturbation theory: The new approach to multi-state multi-reference perturbation theory. The Journal of chemical physics **134**(21) (2011)

[54] Yu, H.-G., Muckerman, J.T.: Mrci calculations of the lowest potential energy surface for ch3oh and direct ab initio dynamics simulations of the o (1d)+ ch4 reaction. The Journal of Physical Chemistry A **108**(41), 8615–8623 (2004)

[55] Chang, A., Lin, S.: A theoretical study of the o (1d)+ ch4 reaction ii. Chemical physics letters **384**(4-6), 229–235 (2004)

[56] DeMore, W.B.: Reaction of o (1d) with hydrocarbons in liquid argon. The Journal of Physical Chemistry **73**(2), 391–395 (1969)

[57] Shu, J., Lin, J.J., Lee, Y.T., Yang, X.: Multiple pathway dynamics of the o (1 d)+ c 2 h 6 reaction: A crossed beam study. The Journal of Chemical Physics **115**(2), 849–857 (2001)

[58] Shu, J., Lin, J.J., Lee, Y.T., Yang, X.: A complete look at a multiple pathway reaction: The reaction of o (1 d) with ethane. The Journal of Chemical Physics **114**(1), 4–7 (2001)

[59] Ashfold, M.N., Ingle, R.A., Karsili, T.N., Zhang, J.: Photoinduced c–h bond fission in prototypical organic molecules and radicals. Physical Chemistry Chemical Physics **21**(26), 13880–13901 (2019)

[60] Okabe, H., McNesby, J.: Vacuum ultraviolet photolysis of ethane: Molecular detachment of hydrogen. The Journal of Chemical Physics **34**(2), 668–669 (1961)

[61] Chang, Y., Yang, J., Chen, Z., Zhang, Z., Yu, Y., Li, Q., He, Z., Zhang, W., Wu, G., Ingle, R.A., *et al.*: Ultraviolet photochemistry of ethane: implications for the atmospheric chemistry of the gas giants. Chemical Science **11**(19), 5089–5097 (2020)

[62] Nguyen, M.T., Matus, M.H., Lester, W.A., Dixon, D.A.: Heats of formation of

triplet ethylene, ethylidene, and acetylene. The Journal of Physical Chemistry A **112**(10), 2082–2087 (2008)

[63] Ma, B., Schaefer III, H.F.: Singlet methylcarbene: Equilibrium geometry or transition state? Journal of the American Chemical Society **116**(8), 3539–3542 (1994)

[64] Leonori, F., Skouteris, D., Petrucci, R., Casavecchia, P., Rosi, M., Balucani, N.: Combined crossed beam and theoretical studies of the c (1d)+ ch4 reaction. The Journal of Chemical Physics **138**(2) (2013)

[65] Cavallotti, C., Leonori, F., Balucani, N., Nevrly, V., Bergeat, A., Falcinelli, S., Vanuzzo, G., Casavecchia, P.: Relevance of the channel leading to formaldehyde+ triplet ethylidene in the o (3p)+ propene reaction under combustion conditions. The journal of physical chemistry letters **5**(23), 4213–4218 (2014)

[66] Janssens, T., Zaera, F.: Chemistry of ethylidene moieties on platinum surfaces: 1, 1-diiodoethane on pt (111). The Journal of Physical Chemistry **100**(33), 14118–14129 (1996)

[67] Sharp, P., Schrock, R.: Multiple metalcarbon bonds: Xiv. preparation of alkylidenetantalum complexes by alkylidene transfer from phosphoranes. the first ethylidene complex and how it decomposes. Journal of Organometallic Chemistry **171**(1), 43–51 (1979)

[68] Datta, S., Davis, H.F.: Direct observation of ethylidene (ch3ch), the elusive high-energy isomer of ethylene. The Journal of Physical Chemistry Letters **11**(24), 10476–10481 (2020)

[69] Hawkins, M., Andrews, L.: Reactions of atomic oxygen with ethene in solid argon. the infrared spectrum of vinyl alcohol. Journal of the American Chemical Society **105**(9), 2523–2530 (1983)

[70] Barbatti, M., Paier, J., Lischka, H.: Photochemistry of ethylene: A multireference configuration interaction investigation of the excited-state energy surfaces. The Journal of chemical physics **121**(23), 11614–11624 (2004)

[71] Minezawa, N., Gordon, M.S.: Optimizing conical intersections by spin- flip density functional theory: application to ethylene. The Journal of Physical Chemistry A **113**(46), 12749–12753 (2009)

[72] Mori, T., Glover, W.J., Schuurman, M.S., Martinez, T.J.: Role of rydberg states in the photochemical dynamics of ethylene. The Journal of Physical Chemistry A **116**(11), 2808–2818 (2012)

[73] Tao, H., Allison, T., Wright, T., Stooke, A., Khurmi, C., Van Tilborg, J., Liu, Y., Falcone, R., Belkacem, A., Martinez, T.: Ultrafast internal conversion in

ethylene. i. the excited state lifetime. The Journal of chemical physics **134**(24) (2011)

[74] Cogan, S., Haas, Y., Zilberg, S.: Intersystem crossing at singlet conical intersections. Journal of Photochemistry and Photobiology A: Chemistry **190**(2-3), 200–206 (2007)

[75] Cui, Q., Morokuma, K., Stanton, J.F.: Ab initio mo studies on the photodissociation of c2h2 from the s1 (1au) state. non-adiabatic effects and st interaction. Chemical physics letters **263**(1-2), 46–53 (1996)

[76] Stanton, J.F., Huang, C.-M., Szalay, P.G.: Stationary points on the s 1 potential energy surface of c2h2. The Journal of chemical physics **101**(1), 356–365 (1994)

[77] Suto, M., Lee, L.: Quantitative photoexcitation and fluorescence studies of c2h2 in vacuum ultraviolet. The Journal of chemical physics **80**(10), 4824–4831 (1984)

[78] Han, J., Ye, C., Suto, M., Lee, L.: Fluorescence from photoexcitation of c2h2 at 50–106 nm. The Journal of chemical physics **90**(8), 4000–4007 (1989)

[79] Campos, A., Boye, S., Brechignac, P., Douin, S., Fellows, C., Shafizadeh, N., Gauyacq, D.: Vacuum–ultraviolet photodissociation of c2h2 via rydberg states: a study of the fluorescent pathways. Chemical physics letters **314**(1-2), 91–100 (1999)

[80] Boyé, S., Campos, A., Douin, S., Fellows, C., Gauyacq, D., Shafizadeh, N., Halvick, P., Boggio-Pasqua, M.: Visible emission from the vibrationally hot c 2 h radical following vacuum-ultraviolet photolysis of acetylene: Experiment and theory. The Journal of chemical physics **116**(20), 8843–8855 (2002)

[81] Ventura, E., Dallos, M., Lischka, H.: The valence-excited states t 1–t 4 and s 1–s 2 of acetylene: A high-level mr-cisd and mr-aqcc investigation of stationary points, potential energy surfaces, and surface crossings. The Journal of chemical physics **118**(4), 1702–1713 (2003)

[82] Shao, Y., Gan, Z., Epifanovsky, E., Gilbert, A.T., Wormit, M., Kussmann, J., Lange, A.W., Behn, A., Deng, J., Feng, X., *et al.*: Advances in molecular quantum chemistry contained in the q-chem 4 program package. Molecular Physics **113**(2), 184–215 (2015)

[83] Mardirossian, N., Head-Gordon, M.: ωb97x-v: A 10-parameter, range-separated hybrid, generalized gradient approximation density functional with nonlocal correlation, designed by a survival-of-the-fittest strategy. Physical Chemistry Chemical Physics **16**(21), 9904–9924 (2014)

[84] Kendall, R.A., Dunning Jr, T.H., Harrison, R.J.: Electron affinities of the first-row atoms revisited. systematic basis sets and wave functions. The Journal of

chemical physics **96**(9), 6796–6806 (1992)

[85] Mallikarjun Sharada, S., Zimmerman, P.M., Bell, A.T., Head-Gordon, M.: Automated transition state searches without evaluating the hessian. Journal of chemical theory and computation **8**(12), 5166–5174 (2012)

[86] Vlaisavljevich, B., Shiozaki, T.: Nuclear energy gradients for internally contracted complete active space second-order perturbation theory: Multistate extensions. Journal of chemical theory and computation **12**(8), 3781–3787 (2016)

[87] Shiozaki, T.: Bagel: brilliantly advanced general electronic-structure library. Wiley Interdisciplinary Reviews: Computational Molecular Science **8**(1), 1331 (2018)

[88] Barbatti, M., Ruckenbauer, M., Plasser, F., Pittner, J., Granucci, G., Persico, M., Lischka, H.: Newton-x: a surface-hopping program for nonadiabatic molecular dynamics. Wiley Interdisciplinary Reviews: Computational Molecular Science **4**(1), 26–33 (2014)

[89] Levchenko, S.V., Krylov, A.I.: Equation-of-motion spin-flip coupled-cluster model with single and double substitutions: Theory and application to cyclobutadiene. The Journal of chemical physics **120**(1), 175–185 (2004)

[90] Krylov, A.I., Sherrill, C.D., Head-Gordon, M.: Excited states theory for optimized orbitals and valence optimized orbitals coupled-cluster doubles models. The Journal of Chemical Physics **113**(16), 6509–6527 (2000)

[91] Stanton, J.F., Bartlett, R.J.: The equation of motion coupled-cluster method. a systematic biorthogonal approach to molecular excitation energies, transition probabilities, and excited state properties. The Journal of chemical physics **98**(9), 7029–7039 (1993)

[92] Krylov, A.I.: Equation-of-motion coupled-cluster methods for open-shell and electronically excited species: The hitchhiker's guide to fock space. Annu. Rev. Phys. Chem. **59**, 433–462 (2008)

[93] Park, J.W., Shiozaki, T.: On-the-fly caspt2 surface-hopping dynamics. Journal of chemical theory and computation **13**(8), 3676–3683 (2017)

[94] Kresse, G., Furthmüller, J.: Efficient iterative schemes for ab initio total-energy calculations using a plane-wave basis set. Physical review B **54**(16), 11169 (1996)

[95] Blöchl, P.E.: Projector augmented-wave method. Physical review B **50**(24), 17953 (1994)

[96] Kresse, G., Joubert, D.: From ultrasoft pseudopotentials to the projector

augmented-wave method. Physical review b **59**(3), 1758 (1999)

[97] Perdew, J.P., Burke, K., Ernzerhof, M.: Generalized gradient approximation made simple. Physical review letters **77**(18), 3865 (1996)

[98] Ernzerhof, M., Scuseria, G.E.: Assessment of the perdew–burke–ernzerhof exchange-correlation functional. The Journal of chemical physics **110**(11), 5029–5036 (1999)

[99] Adamo, C., Barone, V.: Toward reliable density functional methods without adjustable parameters: The pbe0 model. The Journal of chemical physics **110**(13), 6158–6170 (1999)

[100] Tkatchenko, A., DiStasio Jr, R.A., Car, R., Scheffler, M.: Accurate and efficient method for many-body van der waals interactions. Physical review letters **108**(23), 236402 (2012)

[101] Ambrosetti, A., Reilly, A.M., DiStasio, R.A., Tkatchenko, A.: Long-range correlation energy calculated from coupled atomic response functions. The Journal of chemical physics **140**(18) (2014)